Characterization of the CATRiNA neutron detector system

J. F. Perello[a], S. Almaraz-Calderon[a], B. W. Asher[a], L. T. Baby[a], N. Gerken[a], K. Hanselman[a]

[a]*Department of Physics, Florida State University, Tallahassee, Florida 32306, USA*

Abstract

The Compound Array for Transfer Reactions in Nuclear Astrophysics (CATRiNA) is an array of 16 liquid deuterated-benzene (C_6D_6) neutron detectors. The fast-response and pulse-shape-discrimination (PSD) capabilities of liquid scintillators allow for the extraction of neutron energies via time-of-flight and for the identification and separation of neutron/gamma interactions. In addition to these properties, deuterated liquid scintillators have a structured pulse-height spectrum with promising capabilities for neutron spectroscopy. In this paper, we report on the development and characterization of the CATRiNA neutron detector system at Florida State University (FSU). Monte-Carlo simulations and measurements with neutron and γ-ray sources, as well as mono-energetic neutrons (E_n = 2.3 - 7.3 MeV) from in-beam measurements using the ^{7}Li(p,n) reaction, were performed to characterize the detectors. CATRiNA is envisioned to be used to measure several nuclear reactions like (^{3}He,n), (d,n), (p,n), relevant for nuclear structure and nuclear astrophysics studies.

1. Introduction

Neutron detection systems are becoming increasingly necessary in nuclear structure and nuclear astrophysics research. Radioactive beam facilities are probing exotic neutron-rich and neutron-deficient nuclei, where the detection of neutrons in reactions using radioactive beams provides additional information about the properties of such exotic nuclei. Ideally, neutron detection systems are expected to perform neutron spectroscopy and use neutrons to 'tag' other reaction by-products. Efforts in the field have led to the development of large sets of neutron detector systems, for example Refs. [1–3]. Organic scintillators with hydrogen-based compounds (e.g. Anthracene, Stilbene, Benzene) are traditionally the standard for neutron detection due to the high cross section between neutron-proton (n-p) elastic scattering. In particular, liquid scintillators like the NE213 (C_8H_{10}) [4], are useful due to their fast re-

Email address: salmarazcalderon@fsu.edu (S. Almaraz-Calderon)

sponse time (about a few ns), capability to distinguish neutron/gamma (n/γ) interactions within the scintillating material based on the signal's pulse shape, and for extraction of the neutron energy using the Time-of-Flight (ToF) technique.

Deuterated-benzene (C_6D_6) scintillators have recently generated great interest in basic nuclear physics research and related applications [1, 5–7]. Deuterated-benzene scintillators have equivalent response time and pulse-shape discrimination (PSD) capabilities to the standard hydrogen-based scintillators (like the NE213), but with a distinctive peak observed in the light-output spectrum obtained by integrating over the scintillator's light-yield signal when responding to incident mono-energetic-neutrons. This behavior is due to the asymmetry in the cross section of n-d elastic scattering, peaking at backward angles with a maximum energy transfer of 8/9 incident neutron energy (E_n) [5, 6]. This peak is not distinguishable in hydrogen-based detectors due to the isotropic cross section for n-p elastic scattering [5, 6]. The response of the deuterated scintillators to the light-output spectrum opens the possibility to identify mono-energetic neutron groups without relying exclusively on ToF information.

Deuterated scintillator arrays are being used, for example, at Canada's particle accelerator centre (TRIUMF) and University of Michigan (UM). TRIUMF is using the Deuterated Scintillator Array for Neutron Tagging (DESCANT), which consists of 70 deuterated benzene liquid scintillators [1]. DESCANT has been designed to couple with the γ-ray spectrometers TIGRESS and GRIFFIN to enable studies of fusion-evaporation using neutron-rich nuclei by neutron tagging. Additionally, DESCANT will be used to study neutron-emission probabilities of short-lived states above the neutron threshold, which are important for nuclear astrophysical studies. At UM, the University of Michigan Deuterated Scintillator Array (UM-DSA), an array of several deuterated-benzene detectors has been developed [7]. It has been shown that the UM-DSA can be used for neutron spectroscopic studies by only relying on the back-scatter peak information on the light-output spectra to extract neutron energies.

In this paper we describe the development and characterization of the Compound Array for Transfer Reactions in Nuclear Astrophysics (CATRiNA) at Florida State University. CATRiNA is a neutron detector array composed of 16 liquid scintillator detectors based on deuterated-benzene as scintillating material, which has been designed to study nuclear reactions relevant for nuclear structure and nuclear astrophysics studies.

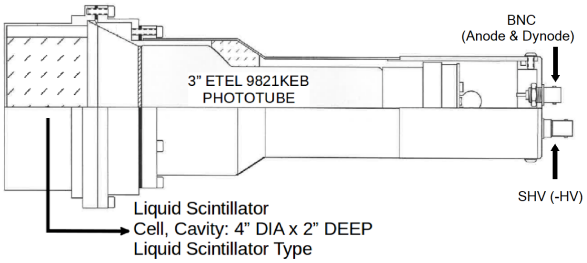

Figure 1: Schematics of the EJ-315 CATRiNA detectors [8]. The C_6D_6 liquid material is contained in a 4" by 2" Al cylinder.

2. CATRiNA

2.1. Detectors and Design

The CATRiNA detectors are of the type EJ-315 manufactured by Eljen Technology [8]. Each EJ-315 detector consists of C_6D_6 scintillating material, which is contained in a 4" diameter × 2" deep cylinder embedded in an aluminum capsule coated with TiO_2 to reduce scintillating light loss and a Pyrex®glass window on the optical end. A nitrogen gas bubble occupies 3% of the volume within the the aluminum capsule along with the liquid scintillating material to reduce light quenching. An acrylic light guide couples the glass window to a ET Enterprise 9821B Photo-Multiplier Tube (PMT) [9]. The PMT has a spectral range of 285-630 nm and the EJ-315 detector has a maximum emission of 450 nm. A schematic of the detectors is shown in Fig. 1.

A 16 channel WIENER MPOD Minicrate High-Voltage (HV) power supply [10] provides about -1700V to each PMT and can be controlled remotely. This allows for fast access to monitor and adjust the HV of the detectors during experiments. The anode output signal from the PMT is sent to a data acquisition system for data analysis.

2.2. Data Acquisition System (DAQ)

For the present characterization, CATRiNA used an analog data acquisition system where signals from the anode of each detector's PMT are sent to a 16 channel Mesytec MCFD module [11]. The MCFD module gives an amplitude and a fast logic signal for each detector. The amplitude signals are delayed by 10.6 m ribbon cable. Both amplitude and logic signals are then split and connected to the two 16-channel banks of a Mesytec MQDC module [12]. The MQDC module allows to specify charge integration time in each bank for PSD, which range from 24 to 219 ns. A logic OR of the fast logic signals is used as a master-trigger and it is sent to a VME controller. The individual fast logic signals are further delayed by about 100 ns and can be used as individual inputs to a CAEN V775 TDC [13] module. To allow coincidence measurements of neutrons, charge particles and/or gamma-rays, this delayed signal can also be used to couple CATRiNA to other detector systems since scintillator detectors are much faster than conventional silicon and germanium detectors. An independent timing-reference signal is derived from the accelerator radio-frequency (RF) signal, which has a 165 ns period and is used as a common stop for the

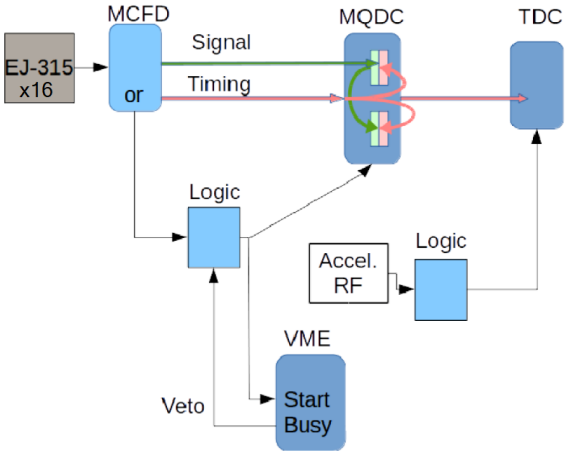

Figure 2: Layout of the data acquisition system used with CATRiNA. All 16 detector's anode signals are sent to the MCFD module. The MCFD splits the input signal and sends as an output the timing and amplitude component to the MQDC module for independent pulse integration. Timing signals from the MCFD are also sent to a CAEN TDC module. The MCFD's OR signal is fed to a LOGIC unit in order to generate a master trigger for the VME controller.

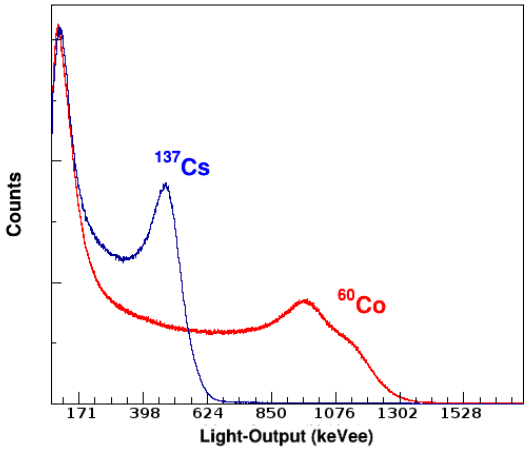

Figure 3: Experimental gamma-ray spectra measured with ^{137}Cs and ^{60}Co sources used for calibration of the CATRiNA detector's light-output.

TDC module. The schematics of the electronics is shown in Fig. 2.

3. Detector Characterization

3.1. γ-ray source measurements

The light response of the detectors was calibrated using two gamma-ray sources, ^{60}Co and ^{137}Cs. Due to a low photo-peak cross section of liquid scintillators, maximum energy transfer is dominated by the Compton effect [4]. The gamma-rays from the radioactive sources will Compton scatter with the electrons of the scintillating material in the detector, producing a Compton edge when maximum gamma energy is transferred to the electrons. A standard calibration unit, "keVee" (keV-electron-equivalent), has been adopted. Here, 1,000 keVee equals the total light-output produced by a 1,000 keV recoiling-electron [14]. A spectrum of the Compton edges measured in the detectors with ^{60}Co and ^{137}Cs gamma-ray sources is shown Fig. 3.

The location of the Compton edge is broadened due to the detector's size and resolution. Placement of the Compton edge was done by simulating the response of the detector with and without detector resolution [15]. For this, a GEANT4 simulation was developed to understand the light-output of the CATRiNA detectors [16]. Simulations using the G4OpticalPhysics, G4EmStandardPhysics, HadronElasticPhysicsHP, and G4DecayPhysics package consisted of a 2"

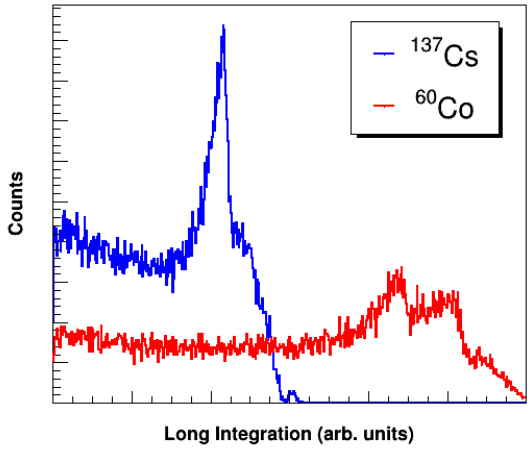

Figure 4: MC simulated spectra for ^{60}Co and ^{137}Cs gamma-ray sources on C_6D_6 material using GEANT4. These simulations do not include detector resolution.

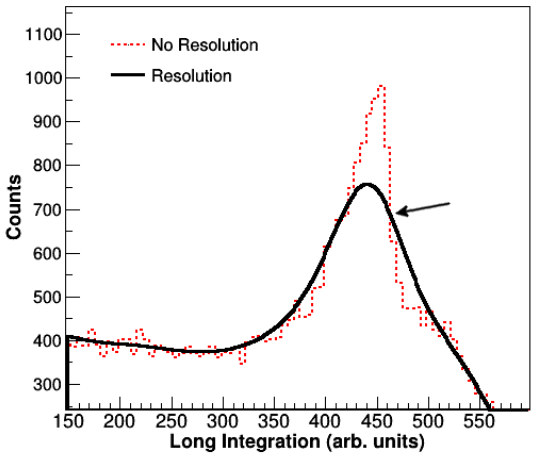

Figure 5: MC simulated spectrum of ^{137}Cs using GEANT4 with and without detector resolution. The intersection at the upper edge of the two peaks (black arrow) is chosen as the location for the Compton edge, which is about 80% maximum height.

long by 4" diameter cylinder of C_6D_6 material, embedded in a 1.5 mm thick aluminum outer casing. Simulated scintillation photons from ^{60}Co and ^{137}Cs gamma-ray sources were compared to the experimental measurements. The simulations of the gamma-ray source spectra without detector resolution are shown in Fig 4. A simulation of a ^{137}Cs spectrum is shown in Fig. 5 with and without detector resolution. Following the procedure of Ref. [15], the location of the Compton edge was placed at the point at which both spectra intersect at the upper edge of the peak (indicated by the black arrow in Fig. 5), usually reported as a percentage of the maximum height of the spectrum with resolution. In this case, the Compton edge was placed at 80% maximum height.

3.2. ^{252}*Cf source measurements*

A pulse-shape discrimination analysis using the charge integration method [17] was performed to separate neutron from gamma-ray interactions in the detectors. A spectrum of the scintillator's light-output can be obtained by integrating over the pulse signals from the PMT's anode. The rise and decay times of the light-output signal emitted from the PMT's anode depends entirely on the scintillating particle type [4]. The decay time of the pulse produced by a gamma interaction is faster in comparison to that of a neutron pulse signal. This is shown in Fig. 6 where different timing gates used for the analysis are also shown. The gates labelled Short, Long and Tail correspond to the integrated

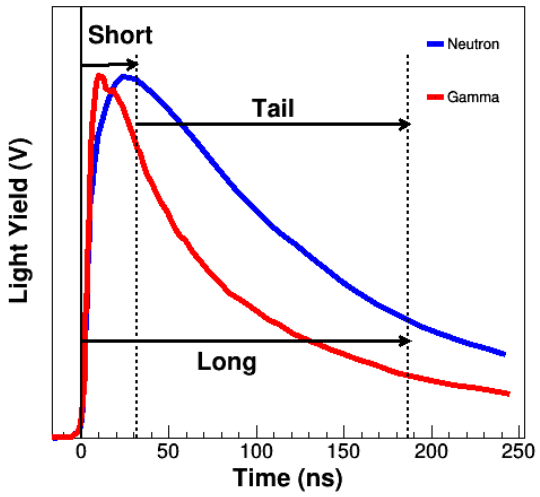

Figure 6: Example of pulse signals emitted by the PMT which are produced by neutron and gamma interactions. The different gate integration times used to discriminate n/γ interactions are also shown.

area (V·ns) and are used to perform PSD in order to distinguish neutron and gamma interactions. The integration times for the Short and Long gates are programmed into the two banks of the MQDC module. The Short gate is chosen to integrate the rise of the pulse, while the Long gate integrates the whole pulse. The Tail integration gate is obtained by subtracting the Short gate from the Long gate.

To find the most favorable integration times for the MQDC module, a ^{252}Cf neutron source was used. By varying the integration times, we found that the optimal values were 32 ns and 187 ns for the Short and Long gate, respectively. The PSD plots shown in the present study were generated by taking the ratio of the gates (Short/Long) and plotting it versus the Long integration value of the pulse. A typical example of a PSD obtained with the ^{252}Cf source can be seen in Fig. 7(a) where neutron and gamma-ray interactions are separated in two well defined groups. It is important to note that the integration times strongly depend on the integration window. For example, if the window opens before the pulse rise, additional time must be given to the Short and Long gate to compensate for this delay.

To quantify the performance of the detectors when separating neutron and gamma interactions, a Figure-of-Merit (FOM) is used. The FOM for each detector was obtained from the 1 dimensional projection of the Short/Long parameter at a given value for the Long parameter, as shown in Fig. 7(b). The FOM is defined as [18, 19]:

$$FOM = \frac{\Delta_C}{\Delta_n + \Delta_\gamma} \quad (1)$$

where Δ_C is the separation between the centroids of the neutron and gamma peaks and Δ_n and Δ_γ are the full-width at half-maximum (FWHM) of the peaks, respectively. A FOM greater than 1 is indicative of a good separation. For the test with a ^{252}Cf source, a FOM of 1.3 for an energy threshold of 250 keVee was achieved for all 16 CATRiNA detectors.

3.3. Measurement of the ^{7}Li(p,n)^{7}Be reaction

Further study of CATRiNA's performance was done by measuring the ^{7}Li(p,n)^{7}Be reaction at the John D. Fox accelerator laboratory at FSU.

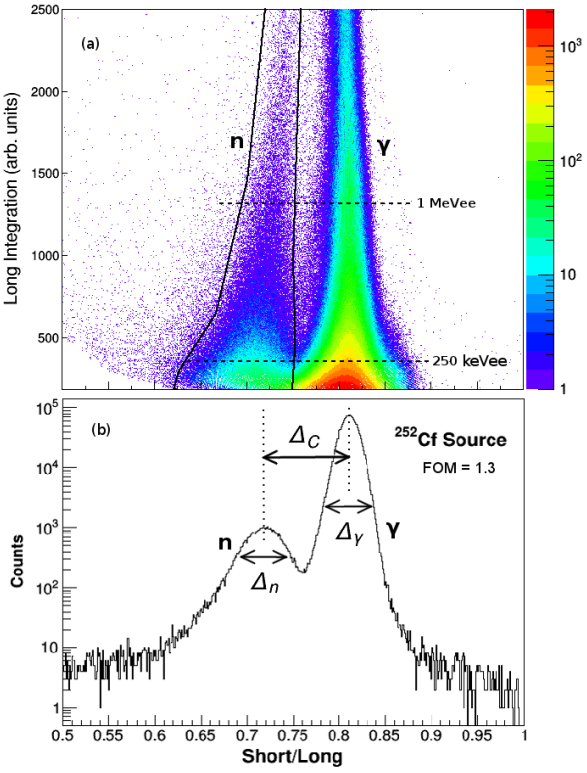

Figure 7: (a) Typical PSD plot obtained with a ^{252}Cf source. Here, the ratio of the gates (Short/Long) is plotted against the Long gate spectrum and is used for n/γ identification. The neutrons appear to the left due to their longer decay time, which corresponds to a larger value for the Long integration. (b) Extraction of FOM. Figure-of-Merit are extracted by projecting the PSD plot onto the x-axis with a given threshold and calculating the width and separation of the n/γ groups according to Eq. 1. For the data shown, a 250 keVee threshold was used and a FOM of 1.3 was extracted, indicating a good n/γ separation.

Experimental data on the excitation function of ^{7}Li(p,n)^{7}Be reaction and the relative cross section of the neutrons from the ground and first excited states of ^{7}Be as a function of proton energy is available in the literature [20] and was used for comparison with the data measured with CATRiNA allowing for the extraction of an experimental efficiency curve of the CATRiNA detectors. In the present experiment, a proton beam from the FN Tandem accelerator was tuned at different energies from 4 to 9 MeV, in 1 MeV increments. The proton beam was pulsed to short bunches of around $\sim$ 2 ns duration with 82.5 ns in between pulses. The proton beam was used to bombard a $\sim$ 200 μg/cm^2 thick ^{7}Li target, which was prepared by evaporating pure ^{7}Li onto a polyvinyl formal resin (formvar) backing at 10-20 Å/s and transported under vacuum to minimize oxidation. Contributions from formvar backing can be neglected since it evaporates once the beam strikes the target. Neutrons from the ground state and first excited state in ^{7}Be populated via the (p,n) reaction were measured in the detectors. The ground state Q-value for the reaction is Q = -1.64 MeV. The first excited state is located at E_{ex1} = 429 keV above the ground state. Contributions of the neutrons from the second and higher excited states in ^{7}Be are negligible in the measurements due to the high excitation energy of the second excited state in ^{7}Be (E_{ex2} = 4570 keV).

In the present configuration, the detectors are

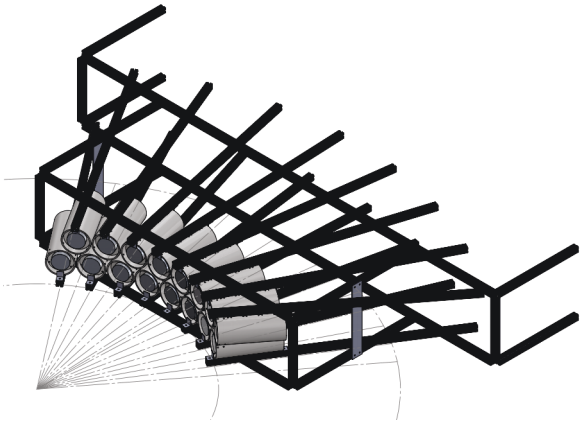

Figure 8: Schematic of the CATRiNA array. The 16 detectors are placed inside a plastic case that can slide and lock to the frame.

placed in two layers, in an array of aluminum material as shown in Fig. 8. Each layer can hold eight detectors with 5° spacing in between. Individual detectors are enclosed in a plastic case and strapped on to the array where they can easily slide and lock between 1 - 2 m from the reaction target to optimize ToF information. CATRiNA has an angular coverage of 40° which allows to obtain angular distributions in a wide range. At the 1 m position, the solid angle coverage of each detector is about 7.8 msr. For the present experiment, CATRiNA was located in target room 1 at the John D. Fox Accelerator Laboratory [21] where the array was suspended by a crane next to the target chamber. The beam-stop was extended from the reaction chamber to minimize neutron background. A silicon detector was also placed in the reaction chamber and was used as a monitor to normalize the beam current using elastic scattering. The silicon detector was added

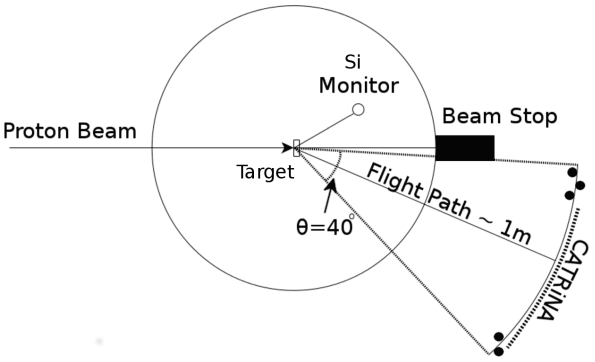

Figure 9: Experimental setup for the measurement of the ^{7}Li(p,n)^{7}Be at the John D. Fox Accelerator Laboratory at FSU.

to the electronics as discussed in Sec. 2.2 via an additional CAEN ADC module. To calculate the dead-time, the before- and after-processing signals were sent to a CAEN scaler module. The experimental setup is shown in Fig. 9.

Neutron energies were extracted using the ToF information from the TDC modules by obtaining the time difference (ΔToF) of the prompt-gamma and neutron peaks coming from the target. To achieve this, the accelerators RF signal was used as a 'stop' signal for the TDC, with the 'start' signal being events registered in the CATRiNA detectors. Energy of the neutrons was then calculated from the target to detector distance and the measured ToF.

4. Results and Discussion

A typical PSD spectrum obtained during the ^{7}Li(p,n)^{7}Be experiment is shown in Fig. 10 where a clear separation between neutrons and gamma rays is visible. The integration parameters used

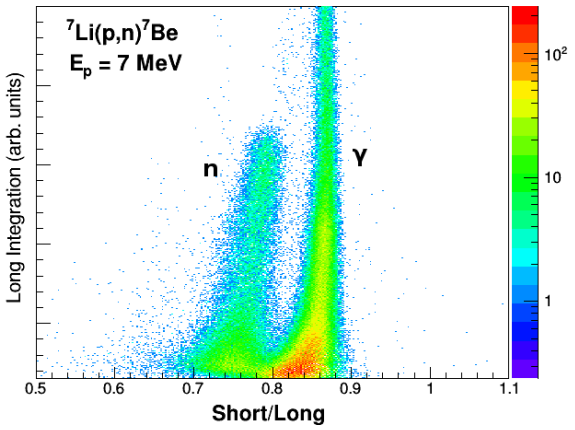

Figure 10: Typical PSD Spectrum of one of the CATRiNA detectors obtained during the reaction measurement of ^{7}Li(p,n)^{7}Be for proton energy of 7 MeV. Groups of n/γ events are clearly separated for further analysis.

were optimized during the measurements with neutron and gamma sources described in Sec. 3.2. From the PSD spectra at each proton energy, the FOM for each detector was extracted as described in Sec. 3.2 for cut-off thresholds of 180 and 250 keVee. The FOM for each neutron energy group of one of the detectors used in the experiment (detector at 10°) is shown in Fig. 11, where they average 1.3 for all the energies covered which indicates a good n/γ separation.

For each detector, the ToF information was gated with the neutron and gamma gates from the PSD spectrum. This allowed to extract the energy of the neutrons via the time difference between the prompt gamma-ray from the interaction of the beam with the target and neutron signals. A typical ToF spectrum for one of the detectors at each

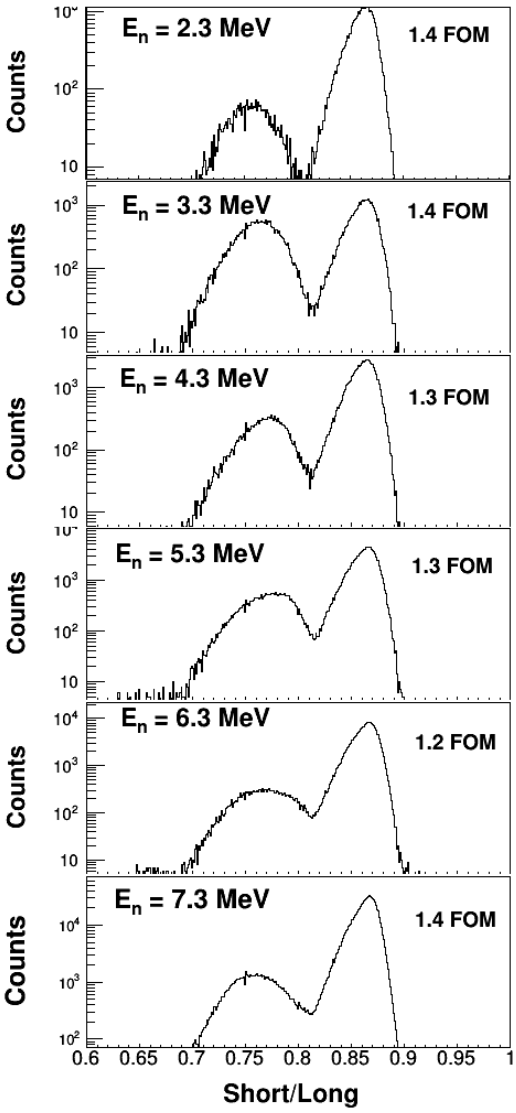

Figure 11: 1-Dimensional plots for different neutron energies of a detector placed at 10° obtained by projecting PSD plots to the x-axis with a 250 keVee threshold. The FWHM and centroid for both neutron peak (left) and gamma peak (right) are calculated by fitting a Gaussian curve. All detectors showed similar behavior.

energy used in the present experiment is shown in Fig. 12.

The neutron ToF spectra are obtained by applying a cut to the neutron group in the PSD plot. The prompt gamma signal is superimposed as reference for ToF calculations. For the first couple of proton energies (E_p = 4 and 5 MeV), neutrons from the ground and first excited state in ^{7}Be are well resolved and the individual cross sections were extracted. For higher proton energies (E_p = 6, 7, 8 and 9 MeV), the cross sections for neutrons from the ground and first excited state in ^{7}Be could not be separated and are extracted together. Background neutrons appeared mainly at higher energies coming from the Faraday cup were also observed in the spectra.

One of the most important aspects of the characterization of CATRiNA was to explore the pulse-height spectra as a function of neutron energy. After the n/γ separation is performed in the PSD spectra, the events in the neutron gate are projected on to the Long integration axis (y-axis) along with a ToF condition, which eliminates most gamma interactions as well as scattered low-energy neutron events. The 1-dimensional projections of the neutron events in one of the detectors for different neutron energies are shown in Fig. 13. It can be seen that there is a distinctive peak that shifts to the right as neutron energy increases. A Gaussian fit to the peaks show that neutron groups with 500 keV

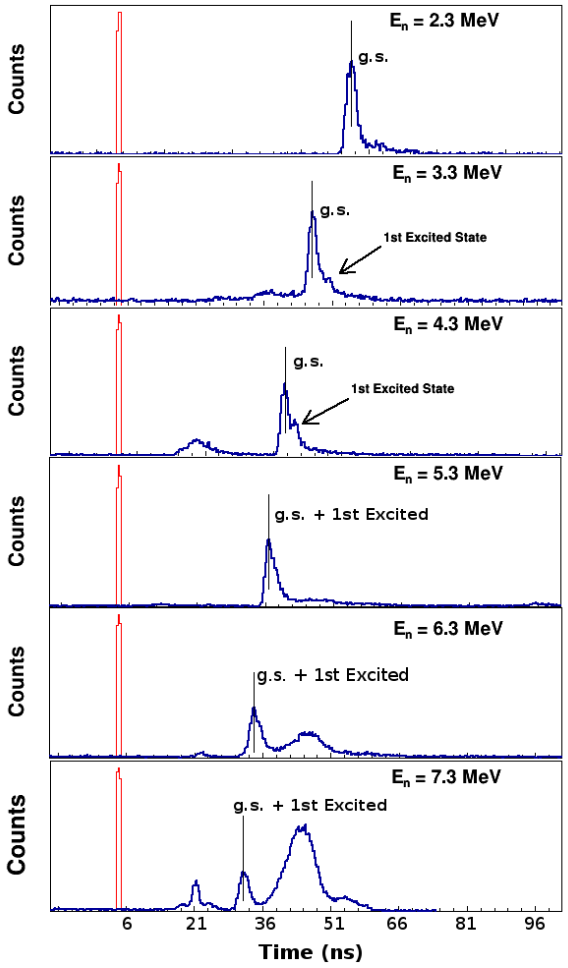

Figure 12: Time-of-Flight spectra of neutrons from the ^{7}Li(p,n)^{7}Be reaction for a CATRiNA detector placed 10° from the beam-axis at forward angles. Neutrons from reactions which populated the ground state of ^{7}Be are marked with a black line and the energies are labelled. For reactions with ground state neutrons of E_n = 4.3-7.3 (E_p = 6-9 MeV), neutrons from the first excited state cannot be resolved. Additionally, neutrons from the target chamber's Faraday cup are seen at higher energies (E_n = 6.3-7.3 MeV). Superimposed is the prompt-gamma signal in red, which was used as reference for ToF calculations.

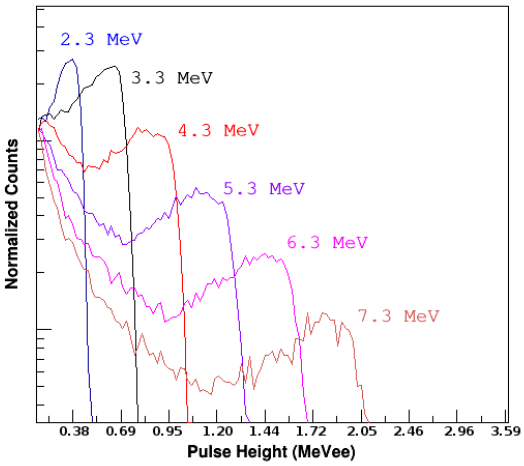

Figure 13: Light-output response of the CATRiNA detectors to quasi-mono-energetic neutrons from the ^{7}Li(p,n) reaction. A distinctive shoulder which shifts to the right as neutron energy increases is observed. For each peak, the energy of the neutron groups is highlighted.

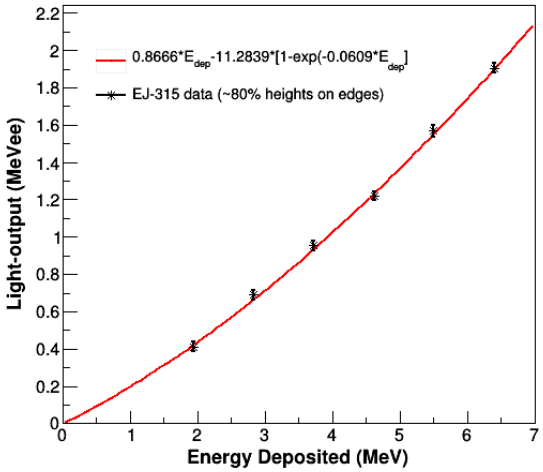

Figure 14: Measured light-output curve for the CATRiNA detectors fitted with a standard exponential form [22].

difference can be well separated. A light-output curve as a function of the energy deposited (8/9 E_n) for the CATRiNA detectors was extracted and is shown in Fig. 14. The light-output curve is fitted with a standard exponential form given by [22]:

$$L = aE_{dep} - b(1 - e^{-cE_{dep}}), \quad (2)$$

where L is the light-output, E_{dep} is the energy deposited and a, b and c are adjustable parameters. The parameters used in the fit were a = 0.8666, b = 11.2839 and c = 0.0609 and covers all the data points measured.

The pulse-height resolution of the CATRiNA detectors to neutron events was determined as follows according to Ref. [15],

$$R = \frac{1.5(L_{1/2} - L_{max})}{L_{1/2}}. \quad (3)$$

Here, $L_{1/2}$ is the location along the edge of the peak where the value is 50% of the maximum and L_{max} is the location of the maximum. The measured resolution for the neutron peaks observed in Fig. 13 as a function of the pulse-height is shown in Fig. 15. The resolution function is expected to follow a $1/\sqrt{pulseheight}$ trend, as reported by other studies [22, 23], fitting the following functional form to the data:

$$R = \sqrt{\alpha^2 + \frac{\beta^2}{L} + \frac{\gamma^2}{L^2}}, \quad (4)$$

where L is the light-output, α, β and γ are adjustable parameters that describe the transmission of the scintillation light through the detector as well as the electronics noise. In this work, $\alpha = 0.1311, \beta$

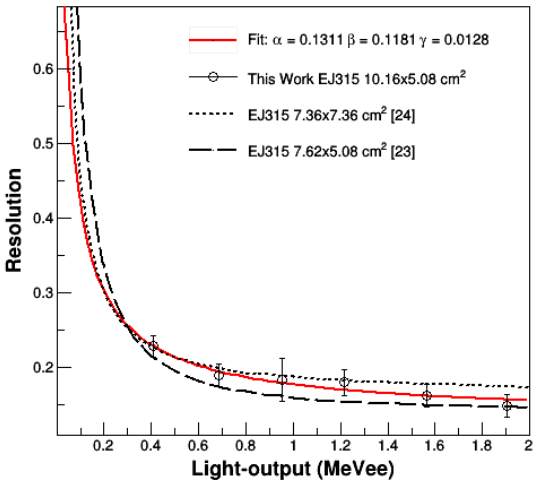

Figure 15: Measured energy resolution of the CATRiNA detectors to neutron events. The resolution is fitted with a functional form given by eq. 4 and shows a comparable trend to works done with similar detector types and sizes [22, 23].

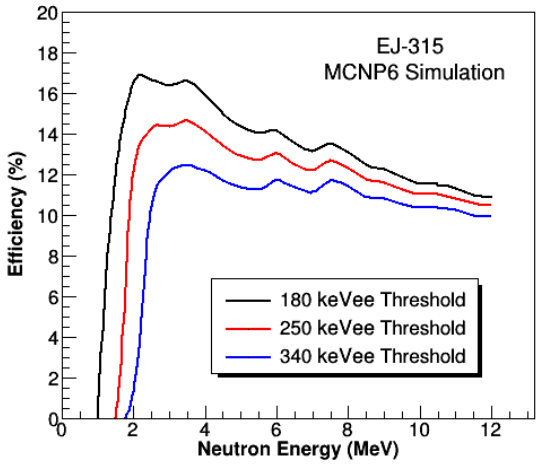

Figure 16: MCNP6 simulated efficiency curve of mono-energetic neutrons at different keVee thresholds.

= 0.1181 and $\gamma = 0.0128$ are the fitted parameters. The results showed a similar behavior to other experiments performed with EJ-315 detectors of sizes 7.36x7.36 cm^2 [23] and 7.62x5.08 cm^2 [22]. The differences found in resolution are attributed to differences in detector size.

A second MC simulation was performed using the neutron-transport code "Monte-Carlo N-Particle Transport Code (MCNP6)" [24]. MCNP6 was used to calculate the efficiency of the detectors and compare to those obtained experimentally. A point source of mono-energetic neutrons was simulated and the threshold was set using a cut-off on the recoil-energy of the deuteron. A conversion between the energy deposited by the neutrons to the deuteron and light-output (in MeVee) is shown in Fig. 14. To obtain the energy deposit information in MCNP6, the PTRAC class was used which provides energy information of every neutron after each collision in the scintillator material. The efficiency of a neutron scintillator detector is threshold dependent, therefore different values were used to understand its behavior. Simulated efficiencies for different thresholds are shown in Fig. 16.

An experimentally measured efficiency curve was extracted by comparing the calculated cross section from the present experiment to data in the literature [20]. Two different thresholds, 180 keVee and 250 keVee, were set on the neutrons in the PSD spectrum. The experimental efficiency curves at 180 and 250 keVee threshold are shown in Fig. 17 and are compared to the MC simulated efficiency curves, finding them in overall good agreement within error bars. The energy spread is less

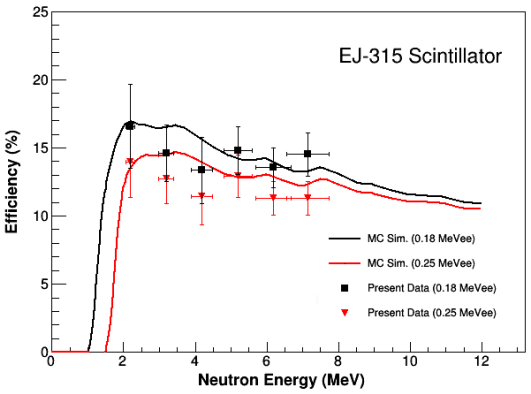

Figure 17: Efficiency curves simulated with MCNP6 for one of the CATRiNA detectors at 180 keVee and 250 keVee threshold plotted along with the extracted experimental efficiencies.

than 8% for the energy range covered, which was calculated by considering the timing resolution of the bunched beam, the thickness of the detectors as well as the uncertainty in the position of the array.

5. Summary and Outlook

We have developed and characterized the CATRiNA neutron detector array at FSU. CATRiNA consist of 16 liquid scintillator detectors based on EJ-315 deuterated benzene (C_6D_6) as scintillating material. Measurements with gamma and neutron sources were performed to optimize the parameters of the MCFD and MQDC modules needed for PSD analysis based on the charge-integration method. The optimized integration times for PSD were found to be 32 ns (Short gate) and 187 ns (Long gate). FOM greater than 1 were consistently obtained for a 250 KeVee threshold with a ^{252}Cf source and 180 KeVee threshold during in-beam experiment for all detectors. Two Monte-Carlo simulations were performed to simulate the response of the CATRiNA detectors and an efficiency curve as a function of neutron energy. A measurement of the The ^{7}Li(p,n)^{7}Be reaction was carried out to study the performance of the detectors to quasi-mono-energetic neutrons and to validate the MC simulations.

Pulse-height analysis showed distinct neutron energy groups for different neutron energies. The analysis and experimental results showed that different neutron energies can be identified without fully relying in ToF if neutron energy differences are larger than ~500 keV for the energy ranged covered. These results opens great possibilities in neutron spectroscopy studies where multiple correlations in PSD, ToF and pulse-height analysis could be combined to optimize and enhance the use of neutron detectors for nuclear reactions relevant in nuclear structure and nuclear astrophysics studies such as (^{3}He,n), (d,n), (p,n). Further developments include the digitization of the data acquisition system and the exploration of different techniques for unfolding the pulse-height signals [7, 22] to improve the resolution of the detectors. The use of CATRiNA in coincidence with other detector systems at FSU, like the Split-Pole Spectrograph as well as with arrays of charge-particles and gamma-rays detectors is also being explored.

Acknowledgements

This work was supported by the Stewardship Science Academic Alliance through the CENTAUR Center of Excellence under grant no. DE-NA0003841, the National Science Foundation under grant no. PHY-1712953 and the State of Florida. We acknowledge the support of D. Caussyn, P.A. Barber and B. Schmidt at the John D. Fox accelerator laboratory and R. Boisseau and J. Aragon at the instrument shop for the fabrication of the CATRiNA array.

[1] P. E. Garrett. Descant – the deuterated scintillator array for neutron tagging. *Hyperfine Interactions*, 225(1):137–141, Jan 2014.

[2] W.A. Peters, S. Ilyushkin, M. Madurga, C. Matei, S.V. Paulauskas, R.K. Grzywacz, D.W. Bardayan, C.R. Brune, J. Allen, J.M. Allen, Z. Bergstrom, J. Blackmon, N.T. Brewer, J.A. Cizewski, P. Copp, M.E. Howard, R. Ikeyama, R.L. Kozub, B. Manning, T.N. Massey, M. Matos, E. Merino, P.D. O'Malley, F. Raiola, C.S. Reingold, F. Sarazin, I. Spassova, S. Taylor, and D. Walter. Performance of the versatile array of neutron detectors at low energy (vandle). *Nuclear Instruments and Methods in Physics Research Section A: Accelerators, Spectrometers, Detectors and Associated Equipment*, 836:122 – 133, 2016.

[3] L.T. Baby, S Kuvin, Ingo Wiedenhoever, M Anastasiou, David Caussyn, K Colbert, N Quails, and D Gay. Resoneut: A detector system for spectroscopy with (d,n) reactions in inverse kinematics. *Nuclear Instruments and Methods in Physics Research Section A: Accelerators, Spectrometers, Detectors and Associated Equipment*, 877, 09 2017.

[4] F.D. Brooks. Development of organic scintillators. *Nuclear Instruments and Methods*, 162(1):477 – 505, 1979.

[5] V. Bildstein, P.E. Garrett, J. Wong, D. Bandyopadhyay, J. Bangay, L. Bianco, B. Hadinia, K.G. Leach, C. Sumithrarachchi, S.F. Ashley, B.P. Crider, M.T. McEllistrem, E.E. Peters, F.M. Prados-Estévez, S.W. Yates, and J.R. Vanhoy. Comparison of deuterated and normal liquid scintillators for fast-neutron detection. *Nuclear Instruments and Methods in Physics Research Section A: Accelerators, Spectrometers, Detectors and Associated Equipment*, 729:188 – 197, 2013.

[6] Chris C. Lawrence, Andreas Enqvist, Marek Flaska, Sara A. Pozzi, and F. D. Becchetti. Comparison of spectrum-unfolding performance of (ej315) and (ej309) liquid scintillators on measured 252cf pulse-height spectra. *Nuclear Instruments and Methods in Physics Research, Section A: Accelerators, Spectrometers, Detectors and Associated Equipment*, 729:924–929, 10 2013.

[7] M. Febbraro, F. D. Becchetti, R. O. Torres-Isea, J. Riggins, C. C. Lawrence, J. J. Kolata, and A. M. Howard. (d,n) proton-transfer reactions on ^{9}Be,^{11} B,^{13} C,^{14,15} N, and ^{19}F and spectroscopic factors at $E_d = 16$ MeV. *Phys. Rev. C*, 96:024613, Aug 2017.

[8] Eljen Technology. Deuterated ej315. https://eljentechnology.com/products/liquid-scintillators/ej-315, Accessed: 2018-04-15.

[9] ET Enterprises Ltd. Photomultipliers. http://www.et-enterprises.com/photomultipliers, Accessed: 2018-04-15.

[10] W-IE-NE-R. Mpod lv/hv. http://www.wiener-d.com/sc/power-supplies/mpod--lvhv/, Accessed: 2018-04-15.

[11] Mesytec. Mcfd-16. https://www.mesytec.com/products/nuclear-physics/MCFD-16.html, Accessed: 2018-04-15.

[12] Mesytec. Mqdc-32. https://www.mesytec.com/products/nuclear-physics/MQDC-32.html, Accessed: 2018-04-15.

[13] CAEN. V775. https://www.caen.it/products/

v775/, Accessed: 2018-04-15.

[14] Mark A. Norsworthy, Marc L. Ruch, Michael C. Hamel, Shaun D. Clarke, Paul A. Hausladen, and Sara A. Pozzi. Light output response of ej-309 liquid organic scintillator to 2.86–3.95 mev carbon recoil ions due to neutron elastic and inelastic scatter. *Nuclear Instruments and Methods in Physics Research Section A: Accelerators, Spectrometers, Detectors and Associated Equipment*, 884:82 – 91, 2018.

[15] G. Dietze and H. Klein. Gamma-calibration of ne 213 scintillation counters. *Nuclear Instruments and Methods in Physics Research*, 193(3):549 – 556, 1982.

[16] S. Agostinelli et al. Geant4—a simulation toolkit. *Nuclear Instruments and Methods*, 506:250 – 303, 2003.

[17] F.D. Brooks. A scintillation counter with neutron and gamma-ray discriminators. *Nuclear Instruments and Methods*, 4(3):151 – 163, 1959.

[18] R.A. Winyard, J.E. Lutkin, and G.W. McBeth. Pulse shape discrimination in inorganic and organic scintillators. i. *Nuclear Instruments and Methods*, 95(1):141 – 153, 1971.

[19] R.A. Winyard and G.W. McBeth. Pulse shape discrimination in inorganic and organic scintillators, ii. *Nuclear Instruments and Methods*, 98(3):525 – 533, 1972.

[20] R. R. Borchers and C. H. Poppe. Neutrons from proton bombardment of lithium. *Phys. Rev.*, 129:2679–2683, Mar 1963.

[21] Florida State University. John d. fox accelerator facility. http://fsunuc.physics.fsu.edu/, Accessed: 2018-04-15.

[22] Chris C. Lawrence, Andreas Enqvist, Marek Flaska, Sara A. Pozzi, A.M. Howard, J.J. Kolata, and F.D. Becchetti. Response characterization for an ej315 deuterated organic-liquid scintillation detector for neutron spectroscopy. *Nuclear Instruments and Methods in Physics Research Section A: Accelerators, Spectrometers, Detectors and Associated Equipment*, 727:21 – 28, 2013.

[23] Haitang Wang, Donald Carter, Thomas N. Massey, and Andreas Enqvist. Neutron light output function and resolution investigation of the deuterated organic liquid scintillator ej-315. *Radiation Measurements*, 89:99 – 106, 2016.

[24] T. Goorley et al. Initial mcnp6 release overview. *Nuclear Technology*, 180:298 – 315, 2012.